Vol. 730: 1–14, 2024
https://doi.org/10.3354/meps14530

MARINE ECOLOGY PROGRESS SERIES
Mar Ecol Prog Ser

Published March 7

Nitrification in the Amazon River plume

Noémie Choisnard*, Theodor Sperlea, Iris Liskow, Maren Voss

Department of Biological Oceanography, Leibniz Institute for Baltic Sea Research Warnemünde, Seestr. 15, 18119 Rostock, Germany

ABSTRACT: The Amazon River delivers high concentrations of nitrate (NO_3^-, ~16 µM) to its estuary, shaping phytoplankton community assemblages in the estuary and up to 1500 km away from the river mouth. Yet NO_3^- production rates via nitrification, a central process of the nitrogen (N) cycle, have never been studied in this region. By combining nitrification rates and classical oceanographic field measurements with the help of a machine-learning model, we highlight for the first time the variability of nitrification rates along the Amazon River plume and discuss potential relationships with environmental variables. The highest nitrification rates observed at the river mouth (up to 302 nmol l^{-1} h^{-1}) co-occurred with high turbidity, nitrite (NO_2^-) and phosphate (PO_4^{3-}) concentrations, consistent with studies documenting high rates in turbid estuaries. Within less than 200 km from the river mouth, nitrification rates drop to minimum values in the plume and NO_3^- is depleted, likely consumed by phytoplankton when the light limitation constraint is lifted. In addition to climate change, the Amazon River catchment is subject to an array of anthropogenic impacts, such as deforestation, mining and damming. Under these pressures, the riverine discharge, turbidity, nutrient load and nitrification rates will likely be altered. This study gives a baseline for a central N-cycle pathway, also broadening our understanding of its control factors in the region, which is crucial for predicting the future of processes relying on the Amazon River discharge.

KEY WORDS: Nitrification · Amazon River · Nitrate · Remineralization · Machine learning · ^{15}N · Tracer

1. INTRODUCTION

Nitrogen (N) is essential for primary production (Howarth 1988), and the quantity and speciation of N not only exerts control on phytoplankton growth, but also on the biotic community composition. For instance, N-rich water columns favour diatoms (Margalef 1978), while depletion of surface N promotes nano- and pico-size species (Hallegraeff 2010). An increase in ammonium (NH_4^+) over nitrate (NO_3^-) supply can cause a similar shift in community composition, leading to harmful blooms (Glibert et al. 2016). Additionally, the speciation of N, i.e. the availability of reduced over oxidized and organic versus inorganic forms of N, is also a forcing factor of key microbial pathways (Devol 2015, Hu et al. 2019, Kuenen 2020). A central process of the N cycle controlling the speciation of oxidized and reduced forms of inorganic N is nitrification.

Nitrification begins with the oxidation of NH_4^+ to nitrite (NO_2^-). This step, considered to be rate-limiting, is carried out by ammonia-oxidizing archaea (e.g. *Nitrosopumilus maritimus*) and bacteria (e.g. *Nitrosomonas* spp.). In addition to NH_4^+, these organisms can also use urea, cyanate and polyamines as substrates, making them flexible and thus expanding their role in dissolved organic N cycling (Damashek et al. 2019, Kitzinger et al. 2019). NO_2^--oxidizing bacteria are primarily responsible for the subsequent oxidation of NO_2^- to NO_3^- in the oxic ocean (Ward 2011) and re-

*Corresponding author: noemie.choisnard@io-warnemuende.de

Publisher: Inter-Research · www.int-res.com

cently, comammox (complete ammonia oxidation) bacteria were found to be capable of fully oxidizing NH_4^+ in estuaries and coastal waters (Xia et al. 2018, Sun et al. 2020). As nitrification is a recycling pathway, it is a key process in the N cycle, as it produces substrate for assimilation, dissimilatory NO_3^- reduction to NH_4^+, anammox and denitrification, thus determining the distribution of N species among the different dissolved inorganic N (DIN) pools.

Nitrification can be regulated by a wide variety of factors, such as temperature, salinity and ambient oxygen concentration, and has long been assumed to only occur below the euphotic zone because of inhibition by light and competition for NH_4^+ in the surface ocean (Merbt et al. 2012, Smith et al. 2014, Wan et al. 2018). But while nitrification is a dominant process in the dark mid-depths of the ocean (Wuchter et al. 2006), there is also increasing proof for nitrifier activity in the euphotic zone, suggesting that new production estimates based on the assumption that NO_3^- is purely allochthonous would be overestimated (Ward 2005, Clark et al. 2007, Smith et al. 2014, Peng et al. 2018, Stephens et al. 2020, Laperriere et al. 2021). Therefore, constraining the underlying regulatory mechanisms and the significance of nitrification for the euphotic zone N budget is key to unravelling the controls on primary production.

This is even more crucial in the case of strongly stratified environments, such as estuaries and river plumes, where nutrient resupply from deeper waters is hampered by the salinity gradient, leading to increasing dependency of surface communities on regenerated forms of N for their growth (Pomeroy 1974, Eppley & Peterson 1979, Azam et al. 1983). But estuaries are diverse ecosystems, with widely varying levels of nutrients (i.e. from low to eutrophic levels), productivity, turbidity and tidal range, complicating the relationships between N supply and productivity (Nixon et al. 1986, Paerl et al. 2014). Thus, understanding rates of N cycle processes, such as nitrification, and their role in comparison to riverine N loads in a variety of estuaries is needed to improve coastal management. However, even though nitrification rates have been measured in a variety of regions (Tang et al. 2023), many coastal ecosystems remain understudied.

The Amazon River estuary is no exception, even though the significant freshwater load (6×10^{15} l yr^{-1}, 16.8 µM DIN; DeMaster & Aller 2001) impacts the biotic community structure and its productivity on the entire area of the shelf (Goes et al. 2014), as well as the biochemistry of surface water as far as the Caribbean (Froelich et al. 1978, Muller-Karger et al. 1988, Coles et al. 2013). During periods of maximum discharge in winter and spring, the Amazon River is even potentially responsible for *Sargassum* blooms in the tropical Atlantic (Aquino et al. 2022). Primary production and carbon export were reported to be high in some of the habitats generated by the plume, where dinitrogen fixation is not significant (Subramaniam et al. 2008, Loick-Wilde et al. 2016), underlining the importance of other sources of N for production in the Amazon River plume. These observations call for improved knowledge about the use and transformation of N species along the river plume, and while biogeochemical models were applied to the region (Stukel et al. 2014, Louchard et al. 2021), there is no proof that remineralization rates are correctly represented. Nitrification rate measurements were carried out in the region in 2019, but only 6 stations were sampled in the northern plume beyond 5° N (Starr et al. 2022). Questions regarding the extent of this process at the river mouth and on the entire Brazilian shelf are therefore still unanswered. Still, quantifying remineralization as nitrification and characterizing its environment both remain challenging, as nitrification may overlap with NO_3^- assimilation and its relationship with environmental variables might be highly non-linear.

Machine-learning algorithms provide a new tool for exploring the components of an ecosystem describable by a large number of features, requiring little time and reasonable computing power. Machine learning has been used to describe intricate ecosystems using the microbial community composition (Cordier et al. 2017, Sperlea et al. 2021, 2022) and made it possible to improve water quality prediction in coastal environments (Deng et al. 2021). Machine-learning algorithms have also been used in the N-cycle field, notably for predicting dinitrogen fixation rates in the ocean (Tang et al. 2019). This tool has been increasingly used in environmental sciences (Sun & Scanlon 2019), as many machine-learning models can handle the highly non-linear relationships prominent in environmental systems.

In the Amazon River plume, the role of nitrification in DIN speciation has never been investigated. Here, we measured bulk nitrification rates from the Amazon River mouth to the most northern part of the plume for the first time. To highlight the main characteristics of environments with the highest nitrification rates along the plume, we applied 7 machine-learning models to our data set. This way, we aimed to (1) quantify the nitrification rates along the Amazon River plume and (2) discuss the role of environmental variables linked to elevated nitrification rates along the Amazon River plume.

2. MATERIALS AND METHODS

2.1. Study site and sample collection

Samples were collected during the M-174 cruise undertaken in April and May 2021, during maximum river discharge, along the Amazon River plume aboard the R/V 'Meteor' (Fig. 1). In total, 18 stations were sampled along the plume, from the river mouth to Bajan waters (15° N), to explore the variability of nitrification as river waters move northward. In this way, we covered several habitats, differing in their sea surface temperature and salinity, as well as the depth of the chlorophyll maximum, mixed layer depth and NO_3^- availability (Pham et al. 2024). These habitats were called riverine (RI), young plume core (YPC), western plume margin (WPM), and modified and oceanic sea water (MOW and OSW, respectively; Fig. 1). Water samples were obtained using a Seabird Electronics SBE-32 rosette mounted with 21 Free Flow bottles of 10 l. Vertical profiles of temperature and salinity, dissolved oxygen, turbidity and fluorescence were obtained from a Seabird Electronics SBE-911plus (SN-0603) CTD, SBE43 dissolved oxygen sensor, D&A OBS-3 turbidity sensor and a WETStar fluorometer, respectively, mounted on the rosette.

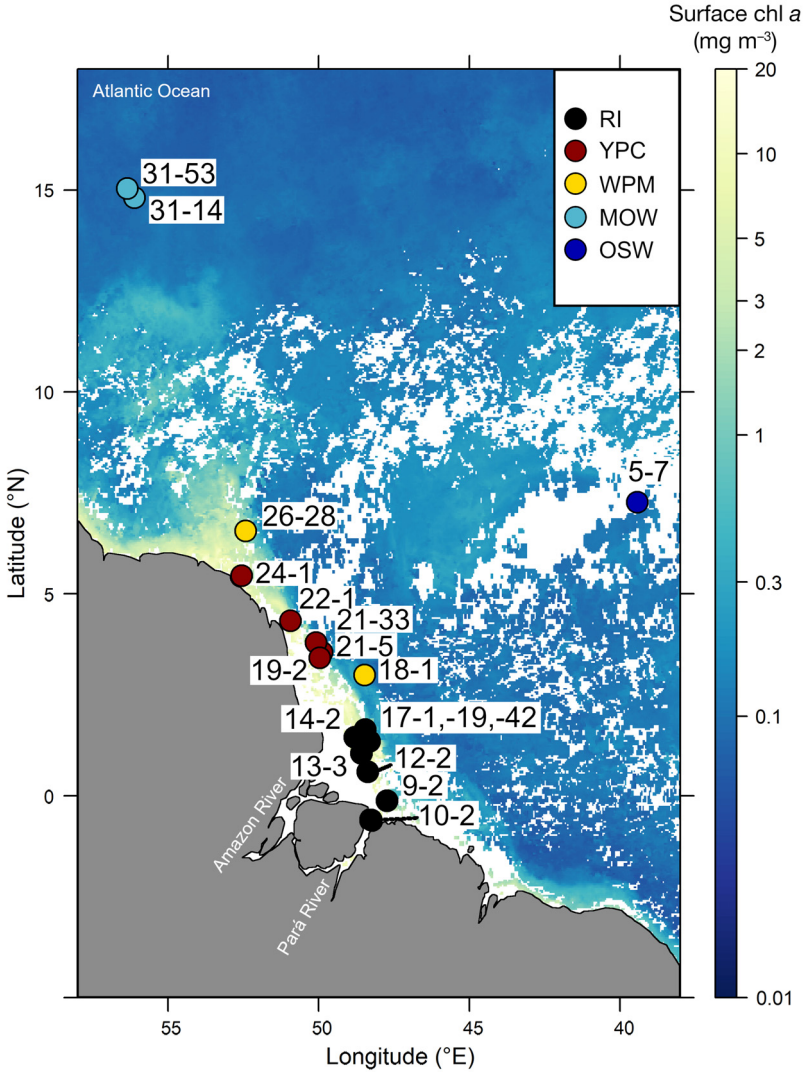

Fig. 1. Study site. The riverine habitat (RI) is located in front of the river mouth and is followed by the young plume core (YPC) and western plume margin (WPM) habitats. The most distant stations are part of the modified oceanic seawater habitat (MOW). An oceanic seawater reference point was also sampled (OSW habitat; Stns 5–7). Surface chl *a* data were obtained for May 2021 from 2014.0 OCI chlorophyll data (AQUA/MODIS, NASA). The plume is discernable, with surface chl *a* values above 5 mg m^{-3}

2.2. Photosynthetically active radiation measurements

The Seabird Electronics device was used to measure photosynthetically active radiation (PAR) throughout the water column. As some casts were not taken during daylight hours, a first selection of all casts measured between 09:00 and 20:30 h was made. A total of 67 casts were taken between 08:00 and 20:00 h and judged suitable for further %PAR (as a percentage of surface irradiance) calculations. The light attenuation coefficient, K_d(PAR), was calculated from a simple linear fit of log-transformed PAR data versus depth (Kirk 1994). The resulting %PAR was calculated as follows:

$$\mathrm{PAR} = \exp\left[-K_d(\mathrm{PAR})z\right] \times 100 \qquad (1)$$

The depth where the %PAR reaches 1% is, by definition, the depth of the euphotic zone.

2.3. Nutrient analysis

Samples for nutrient analysis were filtered (0.2 µm pore size) immediately after collection. Nutrient (silicate [SiO_2], phosphate [PO_4^{3-}], NO_3^-, NO_2^- and NH_4^+) concentrations were determined shortly after filtration, on a continuous flow autoanalyser (QuAAtro, SEAL analytics) following (Grasshoff et al. 1999) and HELCOM guidelines (2014), with a precision of 0.3

(SiO_2), 0.01 (PO_4^{3-}), 0.02 (NO_3^-), 0.006 (NO_2^-) and 0.02 µM (NH_4^+).

2.4. Nitrification rate measurements

Nitrification rates were measured using the ^{15}N-NH_4^+ tracer incubation method (Santoro et al. 2010, Smith et al. 2014, Damashek et al. 2016). Water was collected at each station from 1 to 3 depths (usually at the surface, mid-depth or chlorophyll maximum and bottom or deeper than the chlorophyll maximum; Table S1 in Supplement 1 at www.int-res.com/articles/suppl/m730p001_supp1.xlsx), in triplicate, in 1 l PC bottles and was immediately amended with ^{15}N-NH_4Cl (ISOTEC, Sigma Aldrich, 98 atom%) at approximately 10% of the ambient concentration. Samples for the initial conditions (T_0) were filtered directly after tracer injection onto precombusted (450°C for 4 h) 25 mm GF-075 filters (Advantec, GF-075; 25 mm, nominal pore-size 0.3 µm) while endpoint samples were incubated for 3–6 h before filtration. One set of endpoints was incubated in the dark, at ambient surface temperature, and one set, when the station was sampled during the day, at *in situ* light intensity and temperature. After filtration, 50 ml aliquots of each sample were collected in Falcon tubes and frozen at −20°C until analysis. During the incubation, the labelled ^{15}N-NH_4^+ was converted into ^{15}N-NO_2^- and ^{15}N-NO_3^- (^{15}N-NOx), which was analyzed using the bacterial denitrifier method (Sigman et al. 2001). Samples with a NOx concentration above 0.2 µM were run on a Thermo Scientific Delta V Advantage isotope ratio mass spectrometer connected to a PAL autosampler and a Finnigan GasBench II. Nitrate standards (IAEA-N3 and USGS34) emulating sample concentrations were used for calibration, with an uncertainty of 0.2‰. Nitrification rates depend on the amount of tracer added, the size of the NO_2^- + NO_3^- pool and the excess ^{15}N-NOx measured during the incubation time (ΔT) and were calculated as follows (Damashek et al. 2016):

$$NR = \frac{\left[^{15}N_{NOx}\right] \times \frac{\left[NH_4^+\right]_{total}}{\left[^{15}NH_4^+\right]_{added}}}{\Delta T} \quad (2)$$

where NR is nitrification rate (nmol l^{-1} h^{-1}), ^{15}N-NOx is the difference in ^{15}N content (AP, in atom%) of the end (T_F) and the beginning (T_0) samples:

$$\left[^{15}N_{NOx}\right] = \frac{AP^{15}N_{NOxTF} - AP^{15}N_{NOxT0}}{100} \times \left[NO_3^- + NO_2^-\right] \quad (3)$$

This incubation experiment does not discriminate between NH_4^+ oxidation to NO_2^- and further NO_2^- oxidation to NO_3^-. Three samples were re-analyzed after removing all NO_2^- by treatment with sulfamic acid prior to bacterial conversion to N_2O, according to the protocol of Granger & Sigman (2009). We observed that more than 90% of the labelled NH_4^+ injected ended in the NO_2^- pool (Fig. S1 in Supplement 2 at www.int-res.com/articles/suppl/m730p001_supp2.pdf; for all supplemental figures). It is therefore likely that the nitrification rates reported here mainly reflect NH_4^+ oxidation rates.

2.5. Light and dark incubation experiment

At stations sampled during the day (between 09:00 and 20:00 h), incubations of bottles collected in the euphotic zones (depth of < 50 m) were performed in 2 sets. One set was incubated in the dark, to limit potential competition between nitrifiers and phytoplankton, and one set was incubated under *in situ* light conditions. The aim of the experiment was to study the effect of light on bulk nitrification rates along the Amazon River plume. Results were grouped by PAR levels, which were arbitrarily chosen to be less than 1% (outside of the euphotic zone), 1–10%, 10–50% and above 50% PAR. The effect of temperature is assumed to be modest, as little variation (±2°C) was observed in water temperature between the sampled depths (Fig. S2).

2.6. Detection limit of nitrification rates

The detection limit of nitrification rates was determined for every incubation following (Santoro et al. 2013) and is dependent on the ^{15}N enrichment of the substrate pool and the concentration of the product pool. Detection limits for nitrification rates ranged from 0.003 to 0.400 nmol l^{-1} h^{-1} at RI stations and from 0.003 to 0.050 nmol l^{-1} h^{-1} at YPC stations. Stations located in the WPM habitat exhibited detection limits ranging from 0.001 to 0.06 nmol l^{-1} h^{-1}, while MOW and the oligotrophic station OSW had detection limits of 0.001–0.01 and 0.001–0.08 nmol l^{-1} h^{-1}, respectively.

2.7. Statistical analyses

A total of 7 machine-learning models from the R package 'caret' (v.4.6-14; Kuhn 2008) were used to explore the correlations between a set of environmental

variables and bulk, $\log_{10}$-transformed nitrification rates (in nmol l^{-1} h^{-1}): linear model (lm), elasticnet model (enet), random forest (rf), extreme gradient boosting (xgbTree), support vector machines with linear and radial kernel (svmLinear, svmRadial) and *k*-nearest neighbours (knn). Eleven variables were used as input: temperature, oxygen concentrations, fluorescence, turbidity, salinity, particulate organic N (PON), depth and nutrient concentrations (PO_4^{3-}, NO_3^-, NO_2^- and NH_4^+). All variables without missing values were taken into account in this analysis, and 2 variables were excluded (silica and particulate organic carbon concentrations), as they had the same variability as another variable (with salinity and PON, respectively).

To prevent low (n = 45) sample size-related bias and overfitting in algorithm selection, a leave-one-out cross-validation scheme was applied to evaluate models: a separate model was trained for each sample on all the data points except for the sample in question. Then, the fitted model was used to predict the target variable based on the held-out data point. The predictions were collected and compared to the respective measured values to assess the model. As performance metrics, the coefficient of determination (R^2, explained variance), root-mean-square error (RMSE, standard deviation of the residuals) and model average error (MAE, average absolute difference between predicted and original values) were calculated using the 'postResample' function from the R package 'caret' (v.4.6-14; Kuhn 2008).

Two algorithms were selected based on their performance metrics, with a maximal R^2 and minimal RMSE and MAE as indicators of a good fit. For the variable importance analysis, the 'varImp' function ('caret' package v.4.6-14) was used after re-training these 2 algorithms on the entire data set. That way, complex and non-linear relationships between measured variables and bulk nitrification rates could be detected, and all the data was included in the ranking of the variables selected for explaining bulk nitrification rates along the Amazon River plume. The differences among the means of different groups based on the habitats described earlier were explored using Tukey's test for multiple comparisons.

3. RESULTS

3.1. Environmental variables along the Amazon River plume

The 5 plume habitats sampled exhibited different environmental characteristics. Close to the river mouth, the water column showed a strong stratification between 5 and 10 m depth, with potential density increasing from 0 to 25 kg m^{-3} (Fig. 2A). With distance from the river mouth, the water column depth increased and the potential density of the water column became more homogeneous, with a difference of only ~5 kg m^{-3} between the upper and lower layer of the water column (Fig. 2A).

Oxygen was close to saturation (200–250 µM; Fig. 2B) in the upper 10 m along the Amazon River plume. It decreased to 80–100 µM below the halocline (10 m depth) at shallow stations from the RI and YPC habitats, while in more distant habitats, oxygen concentrations started decreasing between 80 and 200 m depth (Fig. 2B).

N species concentrations (NO_3^-, NO_2^- and NH_4^+) were higher in the river mouth (RI habitat), with NO_3^- being at least 10 times higher (up to 18.4 µM) relative to other habitats, while N concentrations were close to oligotrophic conditions (<0.5 µM). The N to phosphorus (P) ratios, calculated from the ratio between NO_3^- and PO_4^{3-} concentrations, revealed that NO_3^- is rapidly depleted, as all but the RI habitats showed N/P values below the Redfield ratio (16/1).

Nitrification rates showed strong spatial variability. In the RI habitat, nitrification rates were homogeneous throughout the water column, while in other habitats along the plume, nitrification rates were close to 0 at the surface and up to 100 times lower than in deeper waters (Fig. 2G).

3.2. Nitrification rates along the Amazon River plume

Bulk nitrification rates also changed along the Amazon River plume. Rates were higher in habitats more strongly influenced by the Amazon River, as they ranged between 301.6 nmol l^{-1} d^{-1} at the river mouth and 0 at more distant habitats (Fig. 3A). The MOW habitat exhibited nitrification rates in the same range as our oceanic reference (OSW habitat), even though the plume's influence was still noticeable at the surface of this habitat, as previously shown in the density profiles (Fig. 2A).

In addition to the apparent spatial variability of bulk nitrification rates, rates also seemed to vary with light conditions (Fig. 3B). In cases where *in situ* %PAR exceeded 50%, bulk nitrification rates in both incubations were close to 0. As the %PAR decreased, bulk nitrification rates measured under dark conditions increased, while the *in situ* light incubation virtually

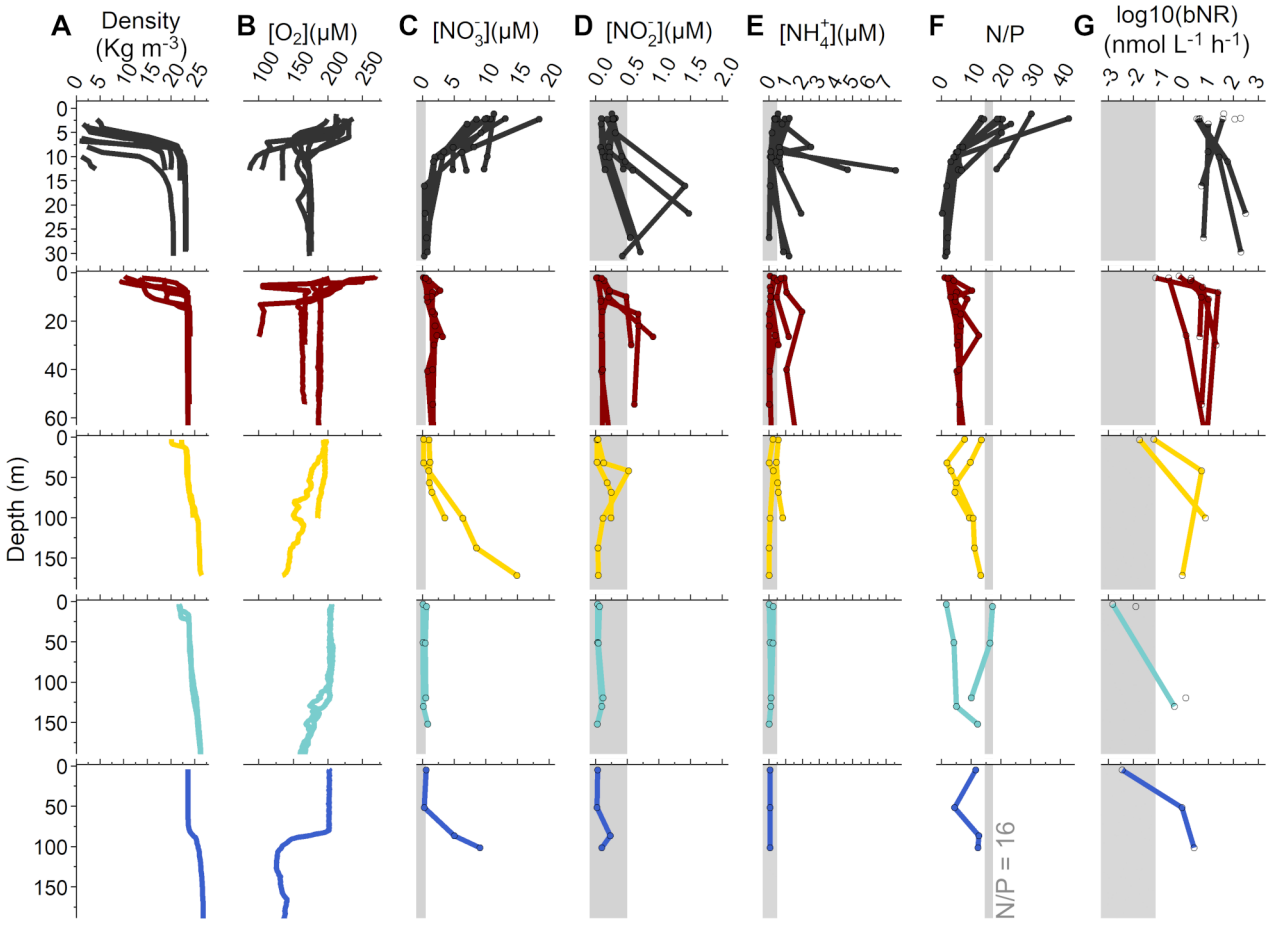

Fig. 2. Diversity of different habitats along the plume, shown by the vertical profiles of (A) density (sigma-theta), (B) dissolved oxygen, (C) NO_3^-, (D) NO_2^-, (E) NH_4^+ and (F) N/P ratios, some variables that might be related to (G) $\log_{10}$-transformed bulk nitrification rates at the RI (black), YPC (red), WPM (yellow), MOW (cyan) and OSW (blue) habitats (see Fig. 1 for habitat abbreviations). Low NO_3^- NO_2^- and NH_4^+ concentrations (<0.5 µM) and rates possibly below the detection limit (<0.4 nmol l^{-1} h^{-1}) are highlighted by the grey area. The grey line on the N/P profiles is set at 16, with values above showing excess of NO_3^- and values below a deficit of NO_3^- relative to PO_4^{3-} according to Redfield ratios (see Section 3.1). Circles indicate sampling depth. For simplification, only the first 0–30 m, 0–60 m or 0–200 m of the water column are presented here

measured no conversion. In light-depleted environments, where %PAR is below 1%, nitrification rates were maximum and rates measured under *in situ* light were in the same order of magnitude as those measured in dark conditions (Fig. 3B).

3.3. Descriptors of habitats with high nitrification rates

To further untangle the relationship between the environmental conditions encountered in each habitat, such as turbidity of the water column, oxygen and nutrient concentrations on the one hand and bulk nitrification rates on the other, we applied a machine-learning feature-importance analysis. To this end, we first identified machine-learning models that best capture this relationship using leave-one-out cross-validation. Models were evaluated using the R^2, RMSE and MAE. The optimal model will produce minimal MAEs and RMSEs and R^2 values close to 1; departures from this optimal value can be either accredited to an ill fit of the model or unobserved variables. We found that the rf, xgbTree and svmRadial outperform the other models, with rf explaining 68% of the variation in the nitrification rate based on the environmental parameters (Table 1). In contrast to the other models used here, the models with high performance are known to be able to model highly non-linear relationships. Therefore, our results stress the importance of non-linear processes in the environmental control of nitrification rates.

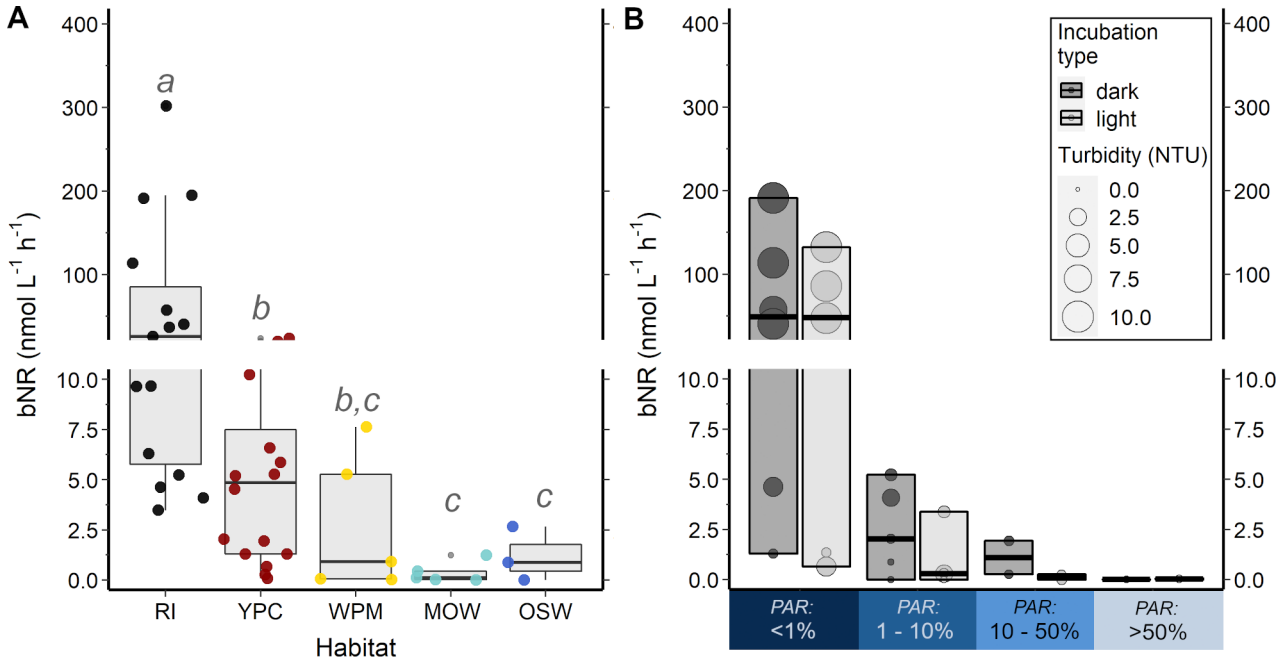

Fig. 3. (A) Bulk nitrification rates (bNR; nmol l^{-1} h^{-1}) vary with habitat. Shared letters above boxes indicate non-significant differences between habitats (Tukey test, $p > 0.05$); habitat abbreviations as in Fig. 1. Boxplots represent the interquartile range. (B) NR measured under dark and *in situ* PAR conditions. The turbidity of each sample is represented by the size of the marker. In both panels and for each box, the median is represented with a bold line

Table 1. Averaged performance metrics (R^2, root-mean-square error [RMSE] and model average error [MAE]) of the 7 machine-learning models applied. lm: linear model; enet: elasticnet model; rf: random forest; xgbTree: extreme gradient boosting; svmLinear and svmRadial: support vector machines with linear and radial kernel, respectively; and knn: *k*-nearest neighbour

Model	R^2	RMSE (nmol l^{-1} h^{-1})	MAE (nmol l^{-1} h^{-1})
lm	0.39	15.00	7.89
enet	0.42	10.81	6.46
rf	0.68	6.04	3.67
xgbTree	0.65	6.29	3.74
svmLinear	0.30	16.18	8.92
svmRadial	0.59	7.89	4.13
knn	0.33	13.17	6.98

Applying feature-importance analysis to the most performant model (rf), we found that NO_2^- and PO_4^{3-} concentrations as well as turbidity and fluorescence are the variables that best describe environments with high bulk nitrification rates (Fig. 4), as higher NO_2^- and PO_4^{3-} concentrations and turbidity co-occur with high bulk nitrification rates (Fig. 5). Fluorescence and bulk nitrification rates varied simi-

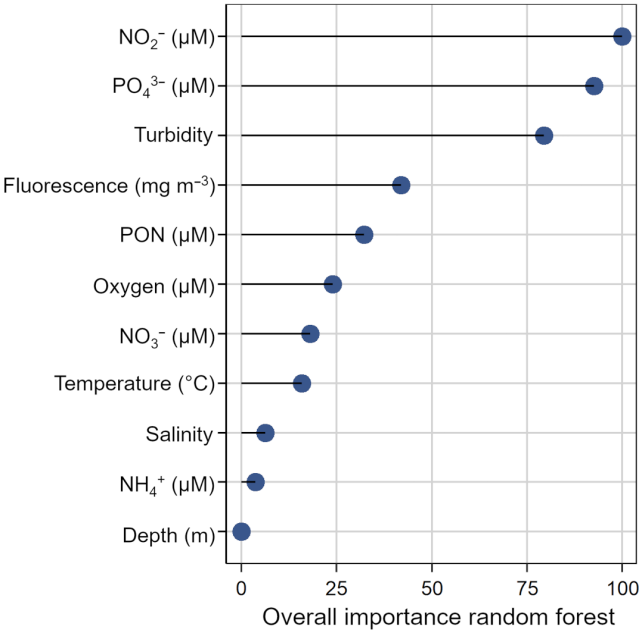

Fig. 4. Ranking of variables used in the random forest model, showing which variables are, according to our model, the best predictor for bulk nitrification rates in the Amazon River plume. The overall importance of each variable was determined by computing the relative influence of each variable on the error of all trees

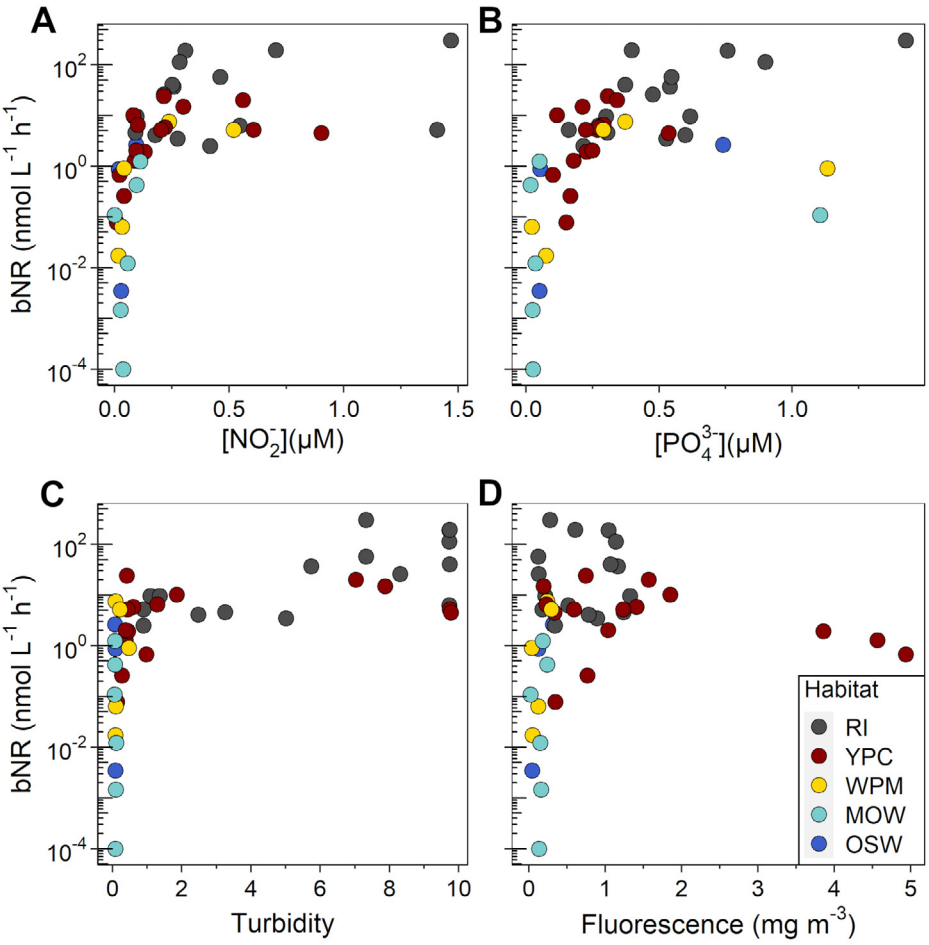

Fig. 5. Concentrations of (A) NO_2^- and (B) PO_4^{3-} as well as (C) turbidity and (D) fluorescence are the variables that had the highest importance for the random forest model. Each of these variables is plotted against bulk nitrification rates and data is coloured by habitat. Note the log scale of the *y*-axis; see Fig. 1 for habitat abbreviations

larly, with nitrification rates increasing together with fluorescence when the latter was below 1 mg m^{-3}. Above that threshold, 3 points were measured with lower nitrification rates (Fig. 5). This ranking of variables is in accordance with the important features identified by the xgbTree model, which also presented NO_2^-, turbidity and PO_4^{3-} as the most important variables (Fig. S3).

4. DISCUSSION

4.1. Nitrification across the Amazon River plume habitats

The Amazon River delivers large quantities of nutrient-rich, turbid freshwater to the estuary. As it is transported northward along the coast and forms the Amazon River plume, the Amazon water undergoes alterations, which are visible in the physical and biochemical properties of the water column. With their characterization of several habitats from the river mouth to 16° N (Fig. 1), Weber et al. (2019) and Pham et al. (2024) have highlighted this diversity, which might impact the N cycle along the Amazon River plume beyond NO_3^- availability and phytoplankton species composition.

In the RI habitat, the freshwater of the Amazon River was encountered over the first 10 m of the shallow water column and was characterized by high NO_3^- (ranging between 3.4 and 18.4 µM) and NH_4^+ concentrations (up to 1.2 µM), and an N/P ratio above 16. As the water travelled and mixed with oceanic waters, the vertical stratification became weaker and the upper water column became depleted in all nutrients, resulting in N/P ratios below Redfield (Fig. 2F). The most distant stations, located around 15° N, belonged to a habitat characterized as MOW

(Pham et al. 2024). Despite the presence of a fine layer of less saline water at the very top of the water column, a fingerprint of riverine influence, N species were depleted at the surface (0.07–0.92 µM of DIN) and this habitat was otherwise indistinguishable from the oceanic seawater habitat (Fig. 2).

Similar to N species, the highest nitrification rates were observed at the river mouth (up to 301.6 nmol l^{-1} h^{-1}; Fig. 3A). By contrast, nitrification rates dropped to less than 10 nmol l^{-1} h^{-1} within 100 km of the river mouth, and ranged between 0 and 2.5 nmol l^{-1} h^{-1} at the most distant stations (Fig. 3A), in accordance with rates measured in the northern plume (Starr et al. 2022). Even if nitrification rates increased with depth at deeper stations, they were still 2 orders of magnitude lower than those observed in the river mouth (Fig. 2G). These results suggest that the Amazon River mouth offers perfect conditions for nitrifiers to thrive, as hypothesized by previous studies (DeMaster & Aller 2001, Aquino et al. 2022).

In fact, nitrification rates measured in the river mouth were as high as those observed in the Chang Jiang River mouth and plume and in the Mississippi River, systems with similar settings (Carini et al. 2010, Hsiao et al. 2014). They were also similar to nitrification rates measured in the Rhône River plume, which had NH_4^+ concentrations about 10 times higher at the time of the study (Bianchi et al. 1999). By contrast, the productive Peruvian upwelling system exhibited nitrification rates about 20 times lower, even though surface NH_4^+ and NO_3^- concentrations were similar to those observed in the Amazon River mouth (Fernández et al. 2009). At more distant and oceanic stations, nitrification rates were in the range of rates observed in the oligotrophic Atlantic Ocean (0.4–7 nmol l^{-1} h^{-1}; Clark et al. 2008). The fairly wide range of nitrification rates along the Amazon River plume and across sites with similar environmental conditions suggests strong variability of the factors potentially forcing nitrification rates.

4.2. Environmental variables linked to elevated nitrification rates

A myriad of variables might have an effect on nitrification rates and the biogeochemistry of an estuary. For example, Damashek et al. (2016), reported strong positive correlations of NH_4^+ and suspended particulate matter with nitrification rates in San Francisco Bay and across a range of ecosystems (e.g. brackish inland seas, fjords, temperate and tropical estuaries) using linear models. However, controls on nitrification rates might be more complex than simple linear relationships, and these are rarely encountered (Ward 2005, Clark et al. 2008). To overcome this issue, we applied 7 machine-learning models to our data set, encompassing diverse types of relationships between explanatory and response variables.

As expected, the linear models (lm and svmLinear; Table 1) did not perform well and had, together with the knn model, the lowest R^2 and highest RMSE and MAE (Table 1). The linear model had a maximum RMSE of 32.36 ± 2.88 nmol l^{-1} h^{-1}, a value above all rates measured outside of the RI habitat (Fig. 3A), underlining that this type of model is not adequate here. The model that fitted our data best was the rf model, which had the highest R^2 (0.75 ± 0.10; Table 1). With the 11 explanatory variables used, this model was able to explain nitrification rates with a maximum error of 5.37 ± 1.70 nmol l^{-1} h^{-1}. This error represents less than 2% and less than 30% of the maximum nitrification rates measured in the river mouth and YPC habitats, respectively (Fig. 3A).

The variable importance function ranks the explanatory variables used in the rf model according to their importance for the prediction of nitrification rates. Altogether, this model highlighted the importance of NO_2^- and PO_4^{3-} concentrations, as well as turbidity and fluorescence as good descriptors for nitrification rates in the Amazon River mouth and plume (Fig. 4). The turbidity of riverine waters provides a particle-rich and light-limited environment which likely provides an advantage to nitrifiers over phytoplankton for NH_4^+ (Cole & Cloern 1984, Alpine & Cloern 1988, Smith et al. 2014), and in many estuaries, nitrification rates peak in turbid waters (Owens 1986, Berounsky & Nixon 1993, Iriarte et al. 1997, Brion et al. 2000, de Wilde & de Bie 2000, Pakulski et al. 2000, Hsiao et al. 2014). Our extensive analysis indicates that similar conclusions can be drawn in the highly turbid Amazon River mouth environment (Fig. 5C). As distance from the river mouth increases and turbidity decreases to values under 5 NTU, nitrification rates drop by up to 5 orders of magnitude and the link between turbidity and rates disappears, as previously reported for the northern part of the Amazon River plume (Starr et al. 2022).

Turbidity and light are difficult to discriminate, as the concentration of particles leading to elevated turbidity usually results in light attenuation (Fig. 3B). An incubation experiment with samples of varying turbidity under both dark and *in situ* light conditions revealed that elevated nitrification rates were maintained under both dark and *in situ* light levels when turbidity was high and *in situ* %PAR was below 1%,

while under low turbidity and high light levels, nitrification rates under *in situ* light condition dropped to minimum values (Fig. 3B). These results underline the strong negative effect of light on nitrification rates along the Amazon River plume. To determine whether this reflects a light inhibition of nitrifiers or direct competition with phytoplankton for NH_4^+ remains to be assessed. Fluorescence is a proxy for phytoplankton presence, and while some fluorescence was measured at the surface of the most riverine habitat, these measurements were potentially biased by the high concentration of particles. Alternatively, the continuous supply of NH_4^+ from the river mouth could support both the nitrifier and planktonic communities. The highest fluorescence measurements were observed further offshore, in the YPC habitat, and linked to a decrease in nitrification rates by 2 orders of magnitude (Fig. 5D), which could corroborate the hypothesis of competition with phytoplankton at higher light levels and lower substrate concentration.

While the elevated turbidity of the river mouth therefore seems to provide a sufficient light attenuation for nitrification to prevail, the high concentration of particles additionally provides high concentrations of substrate, promoting the growth of ammonia-oxidizers as observed in other contexts (Zheng et al. 2017, Kache et al. 2021). In the river mouth where the highest PON concentrations were found, particle-associated ammonia-oxidizing archaea and nitrite-oxidizing bacteria were at least threefold more abundant than free-living ones (Satinsky et al. 2015, 2017). Further offshore, in the Amazon River plume, free-living cells accounted for more than 90% of the metatranscriptome (Satinsky et al. 2014), and when looking at the PON fraction of particles, no correlation with nitrification rates was found in the non-riverine habitats (YPC, WPM, MOW and OSW). These results suggest that turbidity, or the concentration of particles, holds an additional role in the sole light-protection of nitrifiers in the river mouth and explains the shift between particle-associated nitrifiers in the river mouth to more free-living communities in the plume as previously observed (Satinsky et al. 2015, 2017).

NO_2^- is an intermediate of nitrification that usually accumulates just below the deep chlorophyll maximum (Brzezinski 1988, Dore & Karl 1996, Santoro et al. 2013). In oxygenated waters, this accumulation results in NO_2^- concentrations of 0.01–1 µM (Ward 2008), similar in magnitude to the peak concentrations observed across habitats along the Amazon River plume (0.01–1.47 µM; Fig. 2D). Nitrifier abundance and nitrification rates often peak at the NO_2^- maximum in the ocean (Ward 1987, Ward et al. 1989, Dore & Karl 1996, Santoro et al. 2010, 2013, 2017, Newell et al. 2011, Buchwald & Casciotti 2013, Smith et al. 2016), though rapid nutrient cycling and mixing in coastal zones tend to conceal this relationship (Hsiao et al. 2014, Bronk et al. 2014, Damashek et al. 2016). It is therefore interesting, though not surprising, to find a similar relationship in our data set (Figs. 4 & 5A). The greater NO_2^- concentrations are observed in the RI and YPC habitats (Fig. 2D), usually below the plume layer (>10 m depth) and the euphotic zone, suggesting that neither river runoff nor the excretion of NO_2^- by phytoplankton likely explain the relatively high NO_2^- concentrations observed here, as pointed out in other environments (Buchwald & Casciotti 2013, Santoro et al. 2013). Instead, the observed NO_2^- accumulation in these environments could arise from nitrification, influenced by differences in maximum growth rate, loss rate and substrate affinity of nitrite-oxidizers relative to ammonia-oxidizers (Zakem et al. 2018) but also from mesoscale turbulences (Lévy et al. 2014, Liu et al. 2023). In the Amazon River plume, the increasing mixing between the river plume layer and the more saline water below as the water moves northward could partly explain the decrease in NO_2^--peak between riverine habitats and more oceanic ones.

Another nutrient, PO_4^{3-}, presented variability similar to nitrification rates, with high concentrations co-occurring with high nitrification rates in the river mouth (Fig. 5B). The Amazon River delivers substantial amounts of PO_4^{3-} to the river mouth (~0.7 µM; Demaster & Pope 1996), and release of PO_4^{3-} from particle desorption and degradation during mixing in the estuary supplies similar concentrations to the water column (Chase & Sayles 1980, Fox et al. 1986). Consequently, most habitats along the Amazon River plume do not seem to be P-limited. PO_4^{3-} concentrations range between 0.2 and 1.0 µM (Benitez-Nelson 2000), with the highest concentrations found in the river mouth. While this co-occurrence might solely be a coincidence, nitrifiers have also been shown to have a similar affinity for PO_4^{3-} as bacterioplankton (Tanaka et al. 2003), together with a strong dependency on P turnover rates. Additionally, recent microcosm experiments in a eutrophic lake highlighted the potential of inorganic P as a fuel for nitrification (Zhou et al. 2023), and marine nitrifiers have been reported to assimilate 2 mmol of P per mole of NH_4^+ respired (Meador et al. 2020). The higher P concentrations and lower P turnover rates encountered in the Amazon River mouth (Sohm & Capone 2010, Meador et al. 2020) could thus enhance nitrification rates in this habitat.

Conversely, NO_3^-, NH_4^+ concentration and temperature did not hold a strong explanatory power according to this model. Correlations between NH_4^+ and nitrification rates must be interpreted with care. In fact, competition with phytoplankton aside, a strong coupling between NH_4^+ production and oxidation may result in the occurrence of high nitrification rates at lower NH_4^+ concentrations (Carini et al. 2010, Hsiao et al. 2014, Bronk et al. 2014), potentially explaining the lack of a strong relationship in some habitats of the Amazon River plume (Fig. S4). The absence of a relationship between NO_3^- and nitrification rates is also not unexpected. Even though it was reported in many studies summarized by Wan et al. (2018), others have noted the absence of such a relationship (Damashek et al. 2016). Wan et al. (2018) suggested that nitrifiers can outcompete phytoplankton in NO_3^--rich waters thanks to their higher NH_4^+ affinities relative to eukaryotic phytoplankton, which dominate these systems. Unsurprisingly, blooms of large centric diatoms were found at a low-salinity and NO_3^--replete site in the plume, along with the highest expression of the eukaryotic NO_3^- transport gene (Zielinski et al. 2016). It is therefore likely that, similar to NH_4^+, NO_3^- is subject to rapid cycling or mixing, resulting in a concealing of its relationship with nitrification rates (Middelburg & Nieuwenhuize 2001).

5. CONCLUSIONS

This study highlights, for the first time, the significance of nitrification as a crucial process of N cycling in the Amazon River plume. The river mouth presented nitrification rates comparable to other coastal zones and 2 orders of magnitude higher than in the open ocean. With high NO_2^- and PO_4^{3-} concentrations, the Amazon River seems to offer the perfect conditions for nitrifiers to thrive. The high turbidity of its waters probably inhibits phytoplankton growth and activity, easing potential competition for NH_4^+. Within a few 100s of km from the river mouth, the NO_3^- produced is depleted, highlighting the importance of nitrification for supporting phytoplankton growth the moment that light limitation constraints are lifted. The Amazon River estuary seems to be a particularly important site for N cycling. Since the Amazon catchment is undergoing drastic changes, this study gives a baseline for a central N-cycle process, also broadening our understanding of its control factors, which is crucial for predicting the future of this ecosystem.

Acknowledgements. The authors thank the Deutsche Forschungsgemeinschaft (DFG) for funding the MeNARP Project (Metabolism of Nitrogen in the Amazon River Plume, project number VO 487/14-1) and the M174 cruise 'N-Amazon' (funding GPF19-1-13, granted to M.V.) aboard the R/V 'Meteor'. The authors also thank Christian Burmeister (nutrient analyses) and the Captain and Crew of the R/V 'Meteor' (support at sea). The authors are also grateful to Volker Mohrholz, Toralf Heene, Robert Mars, Jens Söder and Ajit Subramaniam for compiling the hydrographic properties of water masses at each sampled station (Mohrholz et al. 2022).

LITERATURE CITED

Alpine AE, Cloern JE (1988) Phytoplankton growth rates in a light-limited environment, San Francisco Bay. Mar Ecol Prog Ser 44:167–173

Aquino R, Noriega C, Mascarenhas A, Costa M and others (2022) Possible Amazonian contribution to *Sargassum* enhancement on the Amazon continental shelf. Sci Total Environ 853:158432

Azam F, Fenchel T, Field JG, Gray JS, Meyer-Reil LA, Thingstad F (1983) The ecological role of water-column microbes in the sea. Mar Ecol Prog Ser 10:257–263

Benitez-Nelson CR (2000) The biogeochemical cycling of phosphorus in marine systems. Earth Sci Rev 51:109–135

Berounsky VM, Nixon SW (1993) Rates of nitrification along an estuarine gradient in Narragansett Bay. Estuaries 16: 718–730

Bianchi M, Feliatra, Lefevre D (1999) Regulation of nitrification in the land–ocean contact area of the Rhône River plume (NW Mediterranean). Aquat Microb Ecol 18: 301–312

Brion N, Billen G, Guézennec L, Ficht A (2000) Distribution of nitrifying activity in the Seine River (France) from Paris to the estuary. Estuaries 23:669–682

Bronk DA, Killberg-Thoreson L, Sipler RE, Mulholland MR and others (2014) Nitrogen uptake and regeneration (ammonium regeneration, nitrification and photoproduction) in waters of the West Florida Shelf prone to blooms of *Karenia brevis*. Harmful Algae 38:50–62

Brzezinski MA (1988) Vertical distribution of ammonium in stratified oligotrophic waters. Limnol Oceanogr 33: 1176–1182

Buchwald C, Casciotti KL (2013) Isotopic ratios of nitrite as tracers of the sources and age of oceanic nitrite. Nat Geosci 6:308–313

Carini SA, McCarthy MJ, Gardner WS (2010) An isotope dilution method to measure nitrification rates in the northern Gulf of Mexico and other eutrophic waters. Cont Shelf Res 30:1795–1801

Chase EM, Sayles FL (1980) Phosphorus in suspended sediments of the Amazon River. Estuar Coast Mar Sci 11: 383–391

Clark DR, Rees AP, Joint I (2007) A method for the determination of nitrification rates in oligotrophic marine seawater by gas chromatography/mass spectrometry. Mar Chem 103:84–96

Clark DR, Rees AP, Joint I (2008) Ammonium regeneration and nitrification rates in the oligotrophic Atlantic Ocean: implications for new production estimates. Limnol Oceanogr 53:52–62

Cole BE, Cloern JE (1984) Significance of biomass and light availability to phytoplankton productivity in San Francisco Bay. Mar Ecol Prog Ser 17:15–24

Coles VJ, Brooks MT, Hopkins J, Stukel MR, Yager PL, Hood RR (2013) The pathways and properties of the Amazon River plume in the tropical North Atlantic Ocean. J Geophys Res Oceans 118:6894–6913

Cordier T, Esling P, Lejzerowicz F, Visco J and others (2017) Predicting the ecological quality status of marine environments from eDNA metabarcoding data using supervised machine learning. Environ Sci Technol 51:9118–9126

Damashek J, Casciotti KL, Francis CA (2016) Variable nitrification rates across environmental gradients in turbid, nutrient-rich estuary waters of San Francisco Bay. Estuaries Coasts 39:1050–1071

Damashek J, Tolar BB, Liu Q, Okotie-Oyekan AO, Wallsgrove NJ, Popp BN, Hollibaugh JT (2019) Microbial oxidation of nitrogen supplied as selected organic nitrogen compounds in the South Atlantic Bight. Limnol Oceanogr 64:982–995

de Wilde HPJ, de Bie MJM (2000) Nitrous oxide in the Schelde estuary: production by nitrification and emission to the atmosphere. Mar Chem 69:203–216

DeMaster DJ, Aller RC (2001) Biogeochemical processes on the Amazon shelf: changes in dissolved and particulate fluxes during river/ocean mixing. In: McClain ME (ed) The biogeochemistry of the Amazon Basin. Oxford University Press, Oxford, p 328–357

Demaster DJ, Pope RH (1996) Nutrient dynamics in Amazon shelf waters: results from AMASSEDS. Cont Shelf Res 16: 263–289

Deng T, Chau KW, Duan HF (2021) Machine learning based marine water quality prediction for coastal hydro-environment management. J Environ Manage 284:112051

Devol AH (2015) Denitrification, anammox, and N_2 production in marine sediments. Annu Rev Mar Sci 7:403–423

Dore JE, Karl DM (1996) Nitrification in the euphotic zone as a source for nitrite, nitrate, and nitrous oxide at Station ALOHA. Limnol Oceanogr 41:1619–1628

Eppley RW, Peterson BJ (1979) Particulate organic matter flux and planktonic new production in the deep ocean. Nature 282:677–680

Fernández C, Farías L, Alcaman ME (2009) Primary production and nitrogen regeneration processes in surface waters of the Peruvian upwelling system. Prog Oceanogr 83:159–168

Fox LE, Sager SL, Wofsy SC (1986) The chemical control of soluble phosphorus in the Amazon estuary. Geochim Cosmochim Acta 50:783–794

Froelich PN Jr, Atwood DK, Giese GS (1978) Influence of Amazon River discharge on surface salinity and dissolved silicate concentration in the Caribbean Sea. Deep-Sea Res 25:735–744

Glibert PM, Wilkerson FP, Dugdale RC, Raven JA and others (2016) Pluses and minuses of ammonium and nitrate uptake and assimilation by phytoplankton and implications for productivity and community composition, with emphasis on nitrogen-enriched conditions. Limnol Oceanogr 61:165–197

Goes JI, do Rosario Gomes H, Chekalyuk AM, Carpenter EJ and others (2014) Influence of the Amazon River discharge on the biogeography of phytoplankton communities in the western tropical North Atlantic. Prog Oceanogr 120:29–40

Granger J, Sigman DM (2009) Removal of nitrite with sulfamic acid for nitrate N and O isotope analysis with the denitrifier method. Rapid Commun Mass Spectrom 23: 3753–3762

Grasshoff K, Kremling K, Ehrhardt M (1999) Methods of seawater analysis. John Wiley & Sons, Weinheim

Hallegraeff GM (2010) Ocean climate change, phytoplankton community responses, and harmful algal blooms: a formidable predictive challenge. J Phycol 46:220–235

Howarth RW (1988) Nutrient limitation of net primary production in marine ecosystems. Annu Rev Ecol Syst 19:89–110

Hsiao SSY, Hsu TC, Liu JW, Xie X and others (2014) Nitrification and its oxygen consumption along the turbid Chang Jiang River plume. Biogeosciences 11:2083–2098

Hu Z, Wessels HJCT, van Alen T, Jetten MSM, Kartal B (2019) Nitric oxide-dependent anaerobic ammonium oxidation. Nat Commun 10:1244

Iriarte A, de Madariaga I, Diez-Garagarza F, Revilla M, Orive E (1997) Primary plankton production, respiration and nitrification in a shallow temperate estuary during summer. J Exp Mar Biol Ecol 208:127–151

Kache S, Bartl I, Wäge-Recchioni J, Voss M (2021) Influence of organic particle addition on nitrification rates and ammonium oxidiser abundances in Baltic seawater. Mar Ecol Prog Ser 674:59–72

Kirk JTO (1994) Light and photosynthesis in aquatic ecosystems. Cambridge University Press, Cambridge

Kitzinger K, Padilla CC, Marchant HK, Hach PF and others (2019) Cyanate and urea are substrates for nitrification by *Thaumarchaeota* in the marine environment. Nat Microbiol 4:234–243

Kuenen JG (2020) Anammox and beyond. Environ Microbiol 22:525–536

Kuhn M (2008) Building predictive models in R using the caret package. J Stat Softw 28:1–26

Laperriere SM, Morando M, Capone DG, Gunderson T, Smith JM, Santoro AE (2021) Nitrification and nitrous oxide dynamics in the Southern California Bight. Limnol Oceanogr 66:1099–1112

Lévy M, Jahn O, Dutkiewicz S, Follows MJ (2014) Phytoplankton diversity and community structure affected by oceanic dispersal and mesoscale turbulence. Limnol Oceanogr Fluids Environ 4:67–84

Liu L, Chen M, Wan XS, Du C and others (2023) Reduced nitrite accumulation at the primary nitrite maximum in the cyclonic eddies in the western North Pacific subtropical gyre. Sci Adv 9:eade2078

Loick-Wilde N, Weber SC, Conroy BJ, Capone DG and others (2016) Nitrogen sources and net growth efficiency of zooplankton in three Amazon River plume food webs. Limnol Oceanogr 61:460–481

Louchard D, Gruber N, Münnich M (2021) The impact of the Amazon on the biological pump and the air–sea CO_2 balance of the Western Tropical Atlantic. Global Biogeochem Cycles 35:e2020GB006818

Margalef R (1978) Life-forms of phytoplankton as survival alternatives in an unstable environment. Oceanol Acta 1: 493–509

Meador TB, Schoffelen N, Ferdelman TG, Rebello O, Khachikyan A, Könneke M (2020) Carbon recycling efficiency and phosphate turnover by marine nitrifying archaea. Sci Adv 6:eaba1799

Merbt SN, Stahl DA, Casamayor EO, Martí E, Nicol GW, Prosser JI (2012) Differential photoinhibition of bacterial and archaeal ammonia oxidation. FEMS Microbiol Lett 327:41–46

Middelburg JJ, Nieuwenhuize J (2001) Nitrogen isotope tracing of dissolved inorganic nitrogen behaviour in tidal estuaries. Estuar Coast Shelf Sci 53:385–391

Mohrholz V, Heene T, Mars R, Söder J, Subramaniam A (2022) Hydrographic properties of water masses in the Amazonas River plume obtained in April/May 2021 by CTD measurements during RV METEOR cruise M174. PANGAEA, https://doi.org/10.1594/PANGAEA.942346

Muller-Karger FE, McClain CR, Richardson PL (1988) The dispersal of the Amazon's water. Nature 333:56–59

Newell SE, Babbin AR, Jayakumar A, Ward BB (2011) Ammonia oxidation rates and nitrification in the Arabian Sea. Global Biogeochem Cycles 25:GB4016

Nixon SW, Oviatt CA, Frithsen J, Sullivan B (1986) Nutrients and the productivity of estuarine and coastal marine ecosystems. J Limnol Soc South Africa 12:43–71

Owens NJP (1986) Estuarine nitrification: A naturally occurring fluidized bed reaction? Estuar Coast Shelf Sci 22: 31–44

Paerl HW, Hall NS, Peierls BL, Rossignol KL (2014) Evolving paradigms and challenges in estuarine and coastal eutrophication dynamics in a culturally and climatically stressed world. Estuaries Coasts 37:243–258

Pakulski JD, Benner R, Whitledge T, Amon R and others (2000) Microbial metabolism and nutrient cycling in the Mississippi and Atchafalaya River plumes. Estuar Coast Shelf Sci 50:173–184

Peng X, Fawcett SE, van Oostende N, Wolf MJ, Marconi D, Sigman DM, Ward BB (2018) Nitrogen uptake and nitrification in the subarctic North Atlantic Ocean. Limnol Oceanogr 63:1462–1487

Pham AH, Choisnard N, Fernández-Carrera A, Subramaniam A and others (2024) Planktonic habitats in the Amazon plume region of the western tropical North Atlantic. Front Mar Sci 11:1287497

Pomeroy LR (1974) The ocean's food web, a changing paradigm. Bioscience 24:499–504

Santoro AE, Casciotti KL, Francis CA (2010) Activity, abundance and diversity of nitrifying archaea and bacteria in the central California Current. Environ Microbiol 12: 1989–2006

Santoro AE, Sakamoto CM, Smith JM, Plant JN and others (2013) Measurements of nitrite production in and around the primary nitrite maximum in the central California Current. Biogeosciences 10:7395–7410

Santoro AE, Saito MA, Goepfert TJ, Lamborg CH, Dupont CL, DiTullio GR (2017) Thaumarchaeal ecotype distributions across the equatorial Pacific Ocean and their potential roles in nitrification and sinking flux attenuation. Limnol Oceanogr 62:1984–2003

Satinsky BM, Zielinski BL, Doherty M, Smith CB and others (2014) The Amazon *continuum* dataset: quantitative metagenomic and metatranscriptomic inventories of the Amazon River plume, June 2010. Microbiome 2:17

Satinsky BM, Fortunato CS, Doherty M, Smith CB and others (2015) Metagenomic and metatranscriptomic inventories of the lower Amazon River, May 2011. Microbiome 3:39

Satinsky BM, Smith CB, Sharma S, Landa M and others (2017) Expression patterns of elemental cycling genes in the Amazon River plume. ISME J 11:1852–1864

Sigman DM, Casciotti KL, Andreani M, Barford C, Galanter M, Böhlke JK (2001) A bacterial method for the nitrogen isotopic analysis of nitrate in seawater and freshwater. Anal Chem 73:4145–4153

Smith JM, Chavez FP, Francis CA (2014) Ammonium uptake by phytoplankton regulates nitrification in the sunlit ocean. PLOS ONE 9:e108173

Smith JM, Damashek J, Chavez FP, Francis CA (2016) Factors influencing nitrification rates and the abundance and transcriptional activity of ammonia-oxidizing microorganisms in the dark northeast Pacific Ocean. Limnol Oceanogr 61:596–609

Sohm JA, Capone DG (2010) Zonal differences in phosphorus pools, turnover and deficiency across the tropical North Atlantic Ocean. Global Biogeochem Cycles 24:GB2008

Sperlea T, Kreuder N, Beisser D, Hattab G, Boenigk J, Heider D (2021) Quantification of the covariation of lake microbiomes and environmental variables using a machine learning-based framework. Mol Ecol 30:2131–2144

Sperlea T, Schenk JP, Dreßler H, Beisser D, Hattab G, Boenigk J, Heider D (2022) The relationship between land cover and microbial community composition in European lakes. Sci Total Environ 825:153732

Starr LD, McCarthy MJ, Hammerschmidt CR, Subramaniam A, Despins MC, Montoya JP, Newell SE (2022) Mercury methylation linked to nitrification in the tropical North Atlantic Ocean. Mar Chem 247:104174

Stephens BM, Wankel SD, Beman JM, Rabines AJ, Allen AE, Aluwihare LI (2020) Euphotic zone nitrification in the California Current Ecosystem. Limnol Oceanogr 65:790–806

Stukel MR, Coles VJ, Brooks MT, Hood RR (2014) Top-down, bottom-up and physical controls on diatom-diazotroph assemblage growth in the Amazon River plume. Biogeosciences 11:3259–3278

Subramaniam A, Yager PL, Carpenter EJ, Mahaffey C and others (2008) Amazon River enhances diazotrophy and carbon sequestration in the tropical North Atlantic Ocean. Proc Natl Acad Sci USA 105:10460–10465

Sun AY, Scanlon BR (2019) How can big data and machine learning benefit environment and water management: a survey of methods, applications, and future directions. Environ Res Lett 14:073001

Sun D, Tang X, Zhao M, Zhang Z and others (2020) Distribution and diversity of comammox *Nitrospira* in coastal wetlands of China. Front Microbiol 11:589268

Tanaka T, Rassoulzadegan F, Thingstad TF (2003) Measurements of phosphate affinity constants and phosphorus release rates from the microbial food web in Villefranche Bay, northwestern Mediterranean. Limnol Oceanogr 48: 1150–1160

Tang W, Li Z, Cassar N (2019) Machine learning estimates of global marine nitrogen fixation. J Geophys Res Biogeosci 124:717–730

Tang W, Ward BB, Beman M, Bristow L and others (2023) Database of nitrification and nitrifiers in the global ocean. Earth Syst Sci Data 15:5039–5077

Wan XS, Sheng HX, Dai M, Zhang Y and others (2018) Ambient nitrate switches the ammonium consumption pathway in the euphotic ocean. Nat Commun 9:915

Ward BB (1987) Nitrogen transformations in the Southern California Bight. Deep-Sea Res A, Oceanogr Res Pap 34: 785–805

Ward BB (2005) Temporal variability in nitrification rates and related biogeochemical factors in Monterey Bay, California, USA. Mar Ecol Prog Ser 292:97–109

Ward BB (2008) Nitrification in marine systems. In: Nitrogen in the marine environment. Elsevier, Amsterdam, p 199–261

Ward BB (2011) Measurement and distribution of nitrification rates in the oceans. Methods Enzymol 486:307–323

Ward BB, Glover HE, Lipschultz F (1989) Chemoautotrophic activity and nitrification in the oxygen minimum zone off Peru. Deep-Sea Res A, Oceanogr Res Pap 36:1031–1051

Weber SC, Subramaniam A, Montoya JP, Doan-Nhu H, Nguyen-Ngoc L, Dippner JW, Voss M (2019) Habitat delineation in highly variable marine environments. Front Mar Sci 6:112

Wuchter C, Abbas B, Coolen MJL, Herfort L and others (2006) Archaeal nitrification in the ocean. Proc Natl Acad Sci USA 103:12317–12322

Xia F, Wang JG, Zhu T, Zou B, Rhee SK, Quan ZX (2018) Ubiquity and diversity of complete ammonia oxidizers (comammox). Appl Environ Microbiol 84:e01390-18

Zakem EJ, Al-Haj A, Church MJ, van Dijken GL and others (2018) Ecological control of nitrite in the upper ocean. Nat Commun 9:1206

Zheng ZZ, Wan X, Xu MN, Hsiao SSY and others (2017) Effects of temperature and particles on nitrification in a eutrophic coastal bay in southern China. J Geophys Res Biogeosci 122:2325–2337

Zhou Z, Liu Y, Wang S, Xiao J, Cao X, Zhou Y, Song C (2023) Interactions between phosphorus enrichment and nitrification accelerate relative nitrogen deficiency during cyanobacterial blooms in a large shallow eutrophic lake. Environ Sci Technol 57:2992–3001

Zielinski BL, Allen AE, Carpenter EJ, Coles VJ and others (2016) Patterns of transcript abundance of eukaryotic biogeochemically-relevant genes in the Amazon River plume. PLOS ONE 11:e0160929

Editorial responsibility: Antonio Bode, A Coruña, Spain
Reviewed by: Y. Zhang and 1 anonymous referee

Submitted: July 10, 2023
Accepted: January 8, 2024
Proofs received from author(s): March 1, 2024